PostPrint. Jing Wei et al., *Journal of Materials Chemistry A*, 2023, **11**, 18146-18157
DOI: 10.1039/D3TA03279E

High-performance carbon-capture membranes developed by (non)solvent-induced nanostructural rearrangement in Nafion

Jing Wei [abcd], **Jing Deng** [e], **Yulei Ma** [abcd], **Zikang Qin** [abcd], **Bangda Wang** [abcd], **Liyuan Deng** *[f], **Richard J. Spontak** [gh] **and Zhongde Dai** *[bcd]

[a]*College of Architecture and Environment, Sichuan University, Chengdu 610065, China*
[b]*National Engineering Research Centre for Flue Gas Desulfurization, Chengdu 610065, China*
[c]*Carbon Neutral Technology Innovation Center of Sichuan, Chengdu 610065, China*
[d]*School of Carbon Neutrality Future Technology, Sichuan University, Chengdu 610065, China. E-mail: zhongde.dai@scu.edu.cn*
[e]*ALTR FLTR Inc., Phoenix, Arizona 85034, USA*
[f]*Department of Chemical Engineering, Norwegian University of Science and Technology, Trondheim, 7491, Norway. E-mail: deng@nt.ntnu.no*
[g]*Department of Chemical & Biomolecular Engineering, North Carolina State University, Raleigh, NC 27695, USA*
[h]*Department of Materials Science & Engineering, North Carolina State University, Raleigh, NC 27695, USA*

Abstract

Membrane materials exhibiting high CO_2 permeability and selectivity are needed for CO_2 capture to mitigate global climate change. In this study, Nafion is dissolved in and cast from *N*-methylpyrrolidone to generate membranes that are subsequently immersed in liquid water to promote nanostructural rearrangement of this amphiphilic polyelectrolyte. Gas permeability results confirm that the CO_2 permeability and CO_2/N_2 selectivity of the membrane both increase significantly (to 472 Barrer and 61, respectively) after such rearrangement and thus exceed the 2008 Robeson upper bound. Transmission electron microscopy and small-angle X-ray scattering reveal that the nanostructure of Nafion is affected by the different processing routes utilized here. In addition, the influence of water vapor on the permeability of a CO_2/N_2 mixture at different relative humidity levels has been examined. These results confirm that the morphology and permeability of Nafion membranes are sensitive to water (as vapor or liquid), which enhances CO_2 transport. Moreover, our findings indicate that (non)solvent-induced nanostructural rearrangement of amphiphilic polyelectrolytes constitutes a largely unexplored, but facile and effective, strategy with broad prospects to improve the CO_2-separation efficacy of carbon-capture polymer membranes.

PostPrint. Jing Wei et al., *Journal of Materials Chemistry A*, 2023, **11**, 18146-18157
DOI: 10.1039/D3TA03279E

1. Introduction

Since fossil-fuel combustion is currently the main source of global energy,[1] CO_2 capture from fossil-fuel power plants constitutes an important avenue to reduce atmospheric CO_2 emissions.[2] Presently, amine absorption is the leading technology intended to capture CO_2 from post-combustion flue gas (mainly composed of CO_2 and N_2),[3] but the cost of this process is almost twice that of power generation.[4] In this context, membrane separation in comparison to traditional CO_2 capture technologies possesses several important advantages: high energy efficiency, physical compactness, relative low cost, and scalability,[5] in addition to demonstrating significant development potential. Among the various materials used to fabricate gas-separation membranes, polymers continue to dominate the gas-separation membrane market due to their low price, facile processability and excellent separation performance.[6] However, a "trade-off" relationship is known[7] to exist between CO_2 permeability and selectivity in conventional polymer membranes that typically rely on bulk chemical modification, solvent exposure or thermal annealing to alter their gas-transport properties. New preparation strategies are, however, being developed[8] to nanoengineer CO_2 separation membranes that simultaneously possess both high CO_2 permeability and selectivity.

Here, we turn our attention to block polymers, which are commonly composed of one or more flexible soft (rubbery) segments and one or more hard (glassy or semi-crystalline) segments.[9] This design inherently relies on the spontaneous self-assembly of the thermodynamically incompatible segments to form a nanostructure that effectively integrates the property advantages of the constituent chemical species. With regard to membranes, the hard segments provide mechanical stability for the material, whereas the soft segments provide pathways for penetrant diffusion.[10] Coexistence of soft and hard microdomains effectively balances mechanical durability and transport performance,[11] which are necessary in gas- and water-separation membranes. In this spirit, the most extensively studied block polymer in membrane technology is Pebax™, a poly(ether-*b*-amide) copolymer commercially available with different degrees of hydrophilicity.[12] Ahmad *et al.*[13] have investigated the effects of different solvents on the CO_2 permeability of mixed-matrix membranes (MMMs) consisting of Pebax-1657 with attapulgite (ATP). Their results indicate that the CO_2 permeability and CO_2/N_2 selectivity of such MMMs prepared with *N*-*N*-dimethylformamide (DMF) and 3 wt% ATP reach 97.2 Barrer and 76, respectively. Under the same conditions, the CO_2 permeability of MMMs cast from *N*-methyl-2-pyrrolidone (NMP) increases to 120 Barrer, while the CO_2/N_2 selectivity concurrently decreases slightly to 69. A poly(ethylene oxide-*b*-butylene terephthalate) copolymer marketed as PolyActive™ likewise possesses promising permeability and selectivity attributes for CO_2 capture.[14] Karunakaran *et al.*[15] have examined CO_2-selective MMMs composed of this copolymer and graphene oxide. The CO_2 permeability of the membrane is reported as 143 Barrer, and the corresponding CO_2/N_2 selectivity is 73. Thus, while the CO_2 separation efficacy of these commercial membranes is comparable, their performance remains below the 2008 Robeson upper bound,[16] which quantifies the trade-off between gas permeability and selectivity.

As mentioned earlier, incompatibility between segments promotes the self-assembly of block polymers during membrane preparation, and the resulting nanoscale morphology generates different transport characteristics.[17] In a previous study, we have investigated the CO_2 transport characteristics of an amphiphilic poly[*tert*-butylstyrene-*b*-(ethylene-*alt*-propylene)-*b*-(styrene-*co*-styrenesulfonate)-*b*-(ethylene-*alt*-propylene)-*b*-*tert*-butylstyrene] pentablock polymer, commercialized as Nexar™, prepared from different solvents.[18] Mineart *et al.*[19] report that the morphology of this polymer is solvent-templatable, and our results reveal that the casting solvent not only strongly affects nanostructural characteristics but also significantly influences the gas-transport properties of the membrane. Moreover, immersion of these as-cast membranes in deionized (DI) water, followed by drying prior to analysis, confirms that the membrane morphology can be drastically altered[20,21] due to selective swelling, thereby promoting substantial improvement in CO_2 permeability (482 Barrer) at a near-constant CO_2/N_2 selectivity (57). These performance levels exceed the Robeson upper bound. This finding, however, further suggests that the morphological details (more specifically, the contiguity of the hydrophilic moiety) of nanostructured amphiphilic polyelectrolyte membranes can be easily altered by immersion in a nonsolvent to enhance the connectivity of hydrophilic channels for CO_2 transport and improved CO_2 separation efficiency.

In recent years, membranes based on sulfonated ionomers have become widely adopted in gas-separation technologies.[22] Among these polymers, Nafion™ is a uniquely sulfonated and fluorinated random copolymer (*cf.* Scheme 1) capable of forming a highly irregular nanostructure wherein hydrophilic channels measure on the order of a few nanometers.[23] Its unique ionic properties reflect the combination of perfluoroethylene ether groups with sulfonate groups and a tetrafluoroethylene (PTFE) skeleton.[24] Exposing Nafion™ to liquid water or water vapor increases the number of water molecules associated with each sulfonate group.[25] Upon hydration, the interconnected network of hydrophilic channels enhances movement of water and ionic species. This polymer is available in a variety of cationic forms to achieve a wide range of conductivity. Due to its low CO_2 permeability (2.0 Barrer) and CO_2/N_2 selectivity (~8–10),[26] however, relatively few studies have investigated its use with regard to CO_2 gas separation. Another of our prior studies has focused on preparing a hybrid membrane for carbon capture by physically mixing Nafion™ with an ionic liquid (IL): 1-butyl-3-methylimidazolium tetrafluoroborate ([Bmim][BF_4]). The outcome demonstrates that the incorporation of 40% wt% [Bmim][BF_4] to Nafion™ increases the permeability of CO_2 from 1.6 Barrer to 75 Barrer. In addition, the introduction of water vapor into the gas feed further enhances the CO_2 permeability to 390 Barrer, which is ~200× higher than that of the neat Nafion™ membrane.[27] This result likewise indicates that the gas-separation performance of Nafion™ can be significantly improved by altering the existing nanoscale morphology, which not only opens up new opportunities for the development of Nafion-based CO_2-capture membranes but is also conducive to broadening their applications more generally in gas separations.

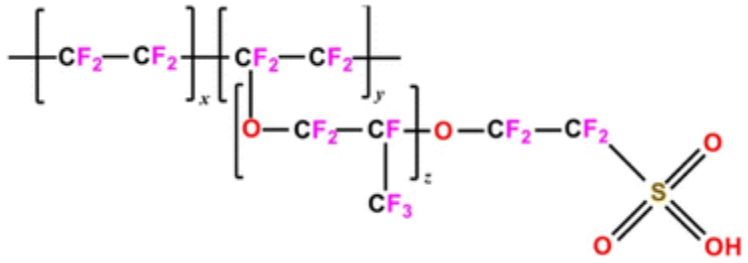

Scheme 1 Chemical structure of Nafion™.

In this study, we employ a liquid nonsolvent (DI water) to induce nanostructural rearrangement of NMP-cast Nafion with the intention of altering the membrane morphology to improve CO_2 separation. Moreover, water vapor is introduced into the feed gas at different relative humidity (RH) conditions to discern the influence of water vapor on both membrane nanostructure and gas transport.

2. Experimental

2.1. Materials

Alcohol-based Nafion solution (5 wt%, D520, total acid capacity 1.03–1.12 Meq. g^{-1}, equivalent weight [EW] = 1000 $g_{polymer}$ mol_{SO3}^{-1}), and extruded Nafion film (~183 μm, Nafion 117, 1100 EW) were obtained from Ion Power (Munich, Germany). Reagent-grade NMP was purchased from Sigma-Aldrich (Buchs, Switzerland) and used without further purification. The DI water was prepared from an in-house water purification system (TE-S20). The gases used in the experiment (at least 99.999% pure) include a CO_2/N_2 mixture, CH_4, CO_2, and N_2, which were all purchased from AGA (Oslo, Norway).

2.2. Membrane fabrication

A predetermined mass of Nafion solution (Nafion-Sol) was magnetically stirred in a round-bottomed flask for at least 30 min and then poured into a glass Petri dish. To keep the membranes uniform and uncracked, they were heated at 80 °C for 100–120 min while covered to reduce the solvent evaporation rate. After each solution was dried in air, the resulting membrane was further dried under vacuum at 60 °C for 6 h before it was analyzed. Nonsolvent-induced nanostructural rearrangement membranes were generated from Nafion-Sol and extruded Nafion (Nafion-Ext) membranes by immersion in DI water for 24 h, followed by vacuum-drying at 35 °C for 24 h before being tested. These membranes are designated as Nafion-Sol-water and Nafion-Ext-water, respectively. Both Nafion-Sol and Nafion-Ext membranes were also dissolved in NMP at 2 wt%, and the solutions were likewise cast in glass Petri dishes as above to yield Nafion-Sol-NMP and Nafion-Ext-NMP membranes. Reported thicknesses ascertained with a Digimatic micrometer (SanLiang, China) are the average of at least 10 measurements over the permeating area.

2.3. Membrane characterization

The thermal behavior of the membranes from 30 to 800 °C was investigated by thermogravimetric analysis (TGA) on a PerkinElmer STA 8000, operated at a heating rate of 10 °C min^{-1}. All measurements were performed under high-purity N_2 (99.999%) at a flow rate of 60 mL min^{-1}. The chemical characteristics of the bulk membranes were examined from 650 to 4000 cm^{-1} by Fourier-transform infrared (FTIR) spectroscopy conducted at ambient temperature in transmission mode on a PerkinElmer Frontier spectrometer. The chemical composition of the membrane surfaces was likewise interrogated at ambient temperature by X-ray photoelectron spectroscopy (XPS) performed on a Kratos XSAM 800 instrument. The internal morphologies of the membranes produced with Nafion-Sol have been characterized by transmission electron microscopy (TEM). To enhance phase contrast, the membranes were exposed to an aqueous solution of lead acetate, which selectively stains the sulfonic acid moieties, as demonstrated elsewhere[19] for a sulfonated block polymer. The stained membranes were subsequently embedded in epoxy resin and ultramicrotomed at ambient temperature to yield electron-transparent sections. Morphological details were imaged on a field-emission FEI Tecnai G2 F20 microscope operated at 200 kV. In addition, small-angle X-ray scattering (SAXS) was conducted with a Xenocs Xeuss 2.0 diffractometer. The sample-to-detector distance and spot size were 2 m and 0.5 × 0.5 mm, respectively, and the wavelength (λ) of the 14 keV beam was 0.087 nm. Intensity profiles were generated as a function of the scattering vector (q), where $q = (4\pi/\lambda)\sin\theta$ and θ is the scattering half-angle, by azimuthally integrating the two-dimensional scattering patterns that were acquired.

Water-vapor uptake tests were performed at ambient temperature and atmospheric pressure. Samples were placed in a closed container filled with saturated water vapor, and the weight of each sample was recorded at different times until a constant value was reached. Water-vapor uptake (Ω) levels were calculated from

$$\Omega = \frac{W_\infty - W_D}{W_D} \times 100\%$$

where W_D and W_∞ represent the weight of the dry and fully saturated membranes, respectively. According to the average value of replicates, the experimental error was less than 5%. Mixed-gas permeability tests were conducted according to the method previously described[18] to elucidate the transport characteristics of CO_2/N_2 gas mixtures at different RH levels. The permeability of CO_2 in the feed gas was determined from

$$P_{CO_2} = \frac{N\left(1 - y_{H_2O}\right) y_{CO_2} L}{A\left(\left\langle P_{CO_2,feed} P_{CO_2,ret} \right\rangle - P_{CO_2,perm}\right)}$$

where N represents the molar flow rate on the permeate side, L is the membrane thickness, A is the permeable area of the membrane, y_{H2O} and y_{CO2} are the mole fractions of water and CO_2 in the permeate, respectively, P_{CO2},feed, P_{CO2},ret and P_{CO2},perm denote the partial pressures of CO_2 in the feed, retentate and permeate, respectively. Gas permeability is expressed throughout

this work in units of Barrer (where 1 Barrer = 10^{-10} cm^3 (STP) cm cm^{-2} s^{-1} cm_{Hg}^{-1}). All permeation results were averaged from triplicates with a standard deviation of less than 10%.

3. Results and discussion

3.1. Morphological analyses

Nafion is an ionic random copolymer capable of forming a poorly defined nanostructure, and its internal ion transport mechanism largely depends on the extent to which its hydrophilic channels are hydrated. It is therefore necessary to understand the nature of the nanostructure that forms in Nafion membranes prepared by different methods. In this study, TEM is used to acquire real-space images of the membrane series consisting of Nafion-Sol, Nafion-Sol-water and Nafion-Sol-NMP membranes. Recalling that the specimens have been selectively stained so that the sulfonated (hydrophilic) regions appear electron-opaque (dark), the results of this analysis are presented for comparison in Fig. 1. As expected from previous TEM studies of Nafion,[28,29] the nanostructure appears generally irregular, apparently composed of co-continuous hydrophilic (sulfonated, dark) and hydrophobic (fluorinated, light) features. According to the morphological analyses of Allen *et al.*[23] and Karan,[30] the hydrophilic channels measure 3–4 nm in size and are anticipated to be fully continuous, which explains the remarkable water and ion transport rates of Nafion in fuel-cell applications.[31] In the images displayed in Fig. 1, we estimate the width of the hydrophilic regions as 2–3 nm, in favorable agreement with prior findings.[32] This observation indicates that the processing histories employed in the preparation of these samples have little impact on the bulk nanostructure of Nafion-Sol, although the different regions appear to become more progressively delineated from Fig. 1a (Nafion-Sol) to Fig. 1c (Nafion-Sol-NMP). While this effect could reflect thickness or staining variation(s) in the TEM samples, it could also be a consequence of solvent-enhanced molecular mobility that serves to improve the spatial separation of the highly incompatible hydrophilic and hydrophobic regions.

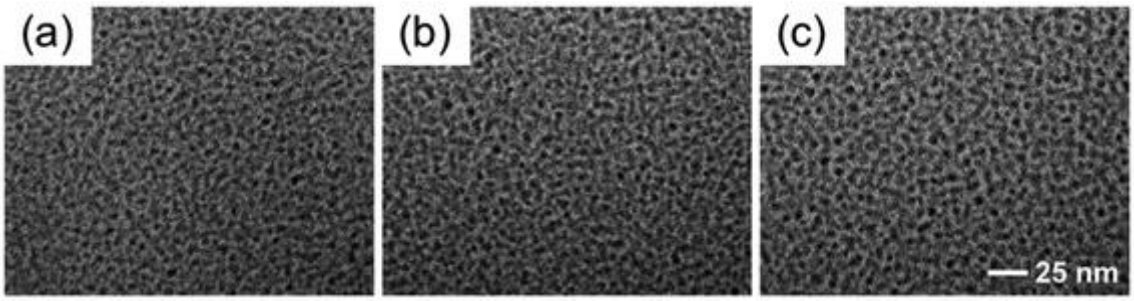

Fig. 1 TEM images of (a) Nafion-Sol, (b) Nafion-Sol-water and (c) Nafion-Sol-NMP membranes. Due to selective staining with Pb acetate, the electron-opaque (dark) features correspond to acid-rich hydrophilic regions. The scale bar included in (c) applies to all the images.

The transfer rate of CO_2 in Nafion membranes clearly depends on the size, shape and connectivity of the hydrophilic regions. While TEM provides valuable spatial information with regard to these morphological features, SAXS affords a more sensitive means to differentiate the morphologies of the membranes prepared in this study. Fig. 2a displays the SAXS profiles

collected from membranes derived from Nafion-Sol (to coincide with the TEM images provided in Fig. 1), whereas those produced from Nafion-Ext are included for comparison in Fig. 2b. The profile for Nafion-Sol in Fig. 2a exhibits a weak peak near 2.2 nm^{-1}, which corresponds to a characteristic spacing (d) of ~2.9 nm according to Bragg's law ($d = 2\pi/q^*$, where q^* represents the scattering vector of interest). This signature spacing is attributed to ionic clusters, previously reported[33] as 2.0 nm, within Nafion. This peak is significantly broadened and shifted to lower q so that the corresponding spacing increases slightly to 3.1 nm upon introduction of DI water in Nafion-Sol-water membranes. Casting from NMP causes a more pronounced reduction in the peak position and a further increase in d to 3.3 nm in Nafion-Sol-NMP membranes. In addition to processing-related shifts in the peak identifying ionic clusters, another feature of Fig. 2a is that the shape of the pre-peak scattering profile of the Nafion-Sol membrane is substantially different from that of the Nafion-Sol-water and Nafion-Sol-NMP membranes, the profiles of which exhibit comparable plateaus from about 0.5 to 1.5 nm^{-1}. Although the precise physical meaning of these scattering shapes is not fully known at this time, it might be related to the difference in spatial delineation discussed with regard to the TEM images in Fig. 1.

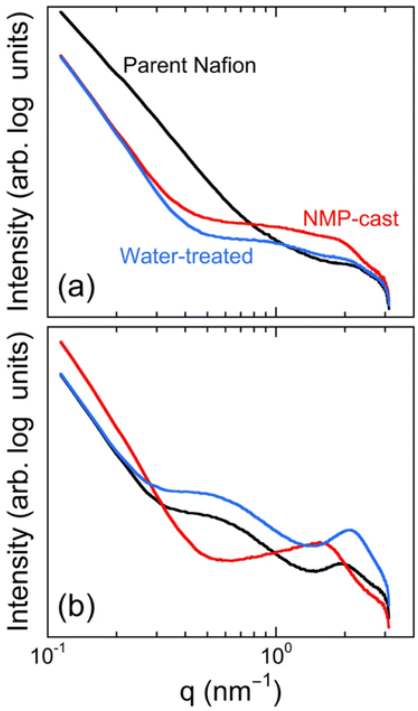

Fig. 2 SAXS profiles of Nafion materials derived from (a) Nafion-Sol and (b) Nafion-Ext. The profiles in each panel are labeled and color-coded according to (a).

In contrast, the features of the scattering profiles acquired from membranes fabricated from Nafion-Ext appear much more clearly defined in Fig. 2b. The pronounced peak reflecting the existence of ionic clusters in the parent Nafion-Ext membrane yields d = 3.3 nm, and this decreases to ~3.0 nm upon hydration in the Nafion-Ext-water membrane. While this value is very similar to that observed in the Nafion-Sol-water membrane in Fig. 2a, the peak in Fig.

2b remains sharp unlike the one broadened in Fig. 2a. The shapes of the SAXS profiles for the Nafion-Ext and Nafion-Ext-water membranes appear qualitatively similar, albeit shifted at $q > 0.2$ nm^{-1}. In this figure, however, the profile obtained from the Nafion-Ext-NMP membrane is markedly different, and the peak attributed to ionic clusters is significantly shifted to lower q, yielding $d = 4.1$ nm. The findings presented in Fig. 2 indicate that variation in process history explored here can have a nontrivial impact on the nanostructural characteristics of Nafion. While the spacing arising from ionic clusters, for example, remains at ∼3 nm for most of the membranes examined here, dissolution of Nafion-Ext in NMP, followed by subsequent solution casting, yields membranes wherein this spacing increases to ∼4 nm. Moreover, the pre-peak SAXS profile shapes reveal that the details of the nanostructures in the Nafion membranes produced here are process-dependent. In prior studies[18,20] of a sulfonated block polymer, exposure to DI water results in profound morphological restructuring and improved CO_2 permeability. Relative to the SAXS profiles collected from the parent Nafion polymers (Nafion-Sol in Fig. 2a and Nafion-Ext in Fig. 2b), immersion in DI water appears to have little effect on the spacing of the pre-existing ionic clusters. The shapes of the SAXS profiles corresponding to membranes subjected to DI water immersion suggest that the hydrophilic channels, which are physically larger than ionic clusters and relate to the pre-peak (medium-q) scattering range, are altered upon exposure to water.

3.2. Physico-chemical analyses

To ascertain the thermal stability of the Nafion membranes generated here, we have performed TGA, and the results are presented in Fig. 3. By assuming that a step-change (not gradual) weight loss of 5 wt% or more identifies the thermal decomposition temperature (T_d) of these materials, measured values of T_d for the Nafion-Sol and Nafion-Ext membranes in Fig. 3a are similar at ∼300 °C. We also note that the decomposition process follows two stages, with the second stage commencing at over 400 °C for each specimen. Casting the polymers from NMP yields the results presented in Fig. 3b. As is evident here, T_d for the Nafion-Ext-NMP film is significantly affected by the casting process, since the first of three decomposition temperatures drops to about 210 °C, whereas the first of only two such temperatures lies at ∼310 °C for the Nafion-Sol-NMP film. The unexpected decrease in T_d for the Nafion-Ext-NMP film likely reflects the presence of residual NMP (with a normal boiling point of 202 °C), confirmed in the Nafion-Sol-NMP film according to XPS analysis (see below), or a solvent-induced change in chain packing (and, by inference, free volume). The high-temperature decomposition process occurs at over 400 °C for each material. In the case of both water-treated materials in Fig. 3c, the first $T_d \approx 315$ °C and the second lies above 400 °C. From *ca.* 300–315 °C to the decomposition temperature above 400 °C, all of the Nafion materials examined here undergo significant mass loss due to the loss of sulfonate groups.[34] Above ∼410 °C, the quality of the material declines sharply as a result of thermal decomposition of the side chain and/or backbone.[35] Although not included in Fig. 3, temperatures near 600 °C promote nearly 100% mass loss, which agrees favorably with previous observations.[27]

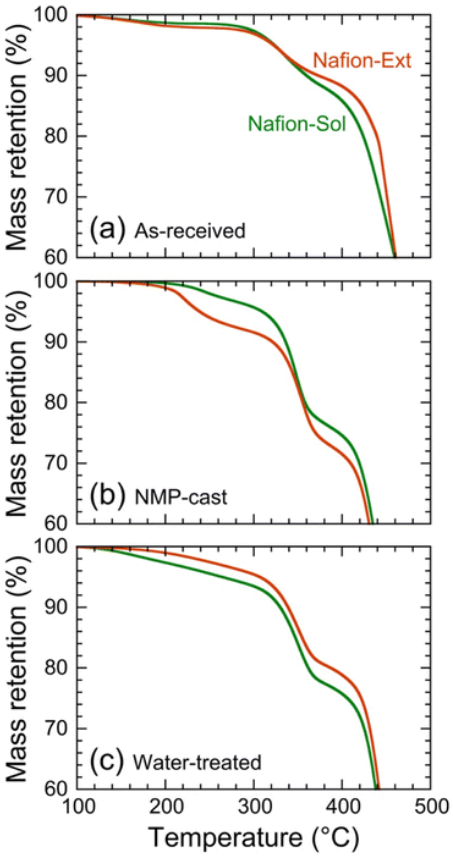

Fig. 3 TGA results acquired from Nafion-Sol (green) and Nafion-Ext (orange) materials prepared according to different protocols: (a) as-received, (b) after NMP casting and (c) after water treatment.

Portions of the FTIR spectra acquired from all the Nafion materials prepared in this study are displayed from 800 to 1400 cm^{-1} in Fig. 4. The primary vibrations of interest with regard to Nafion reside in this so-called "fingerprint" region, and the corresponding bond assignments are listed for convenience in Table 1. The peaks located at 982, 1055, 1144, and 1200 cm^{-1} are representative of Nafion, according to results provided elsewhere.[36,37] In addition, broad peaks observed at ~1710 cm^{-1} and in the region between *ca.* 3000 and 3600 cm^{-1} (data not shown) reflect the bending[38] and stretching[36] vibrations of H_2O and H_3O^+, respectively. As expected, comparison of the FTIR spectra for materials derived from Nafion-Sol and Nafion-Ext reveals the development of no new vibration peaks that would be suggestive of a new chemical bond. Moreover, changes in the positions of the characteristic peaks are negligibly small, indicating that no chemical interactions occur between Nafion and either NMP used as a solvent or water used as a non-solvent in this study. The surface chemical composition and bonding nature of these Nafion materials have also been analyzed by XPS. According to the FTIR analysis, no new chemical interactions transpire during solvent casting from NMP or nanostructural rearrangement of the Nafion membranes, in which case the Nafion-Sol-water membrane is selected here for illustrative purposes. The XPS survey spectrum in Fig. 5a confirms that the Nafion-Sol-water material mainly consists of F, O, C, and S, although N (from NMP) is also present in trace quantity. Peak characteristics have been extracted in high-resolution XPS spectra according to the deconvolution method of Vijayakumar *et al.*[39]

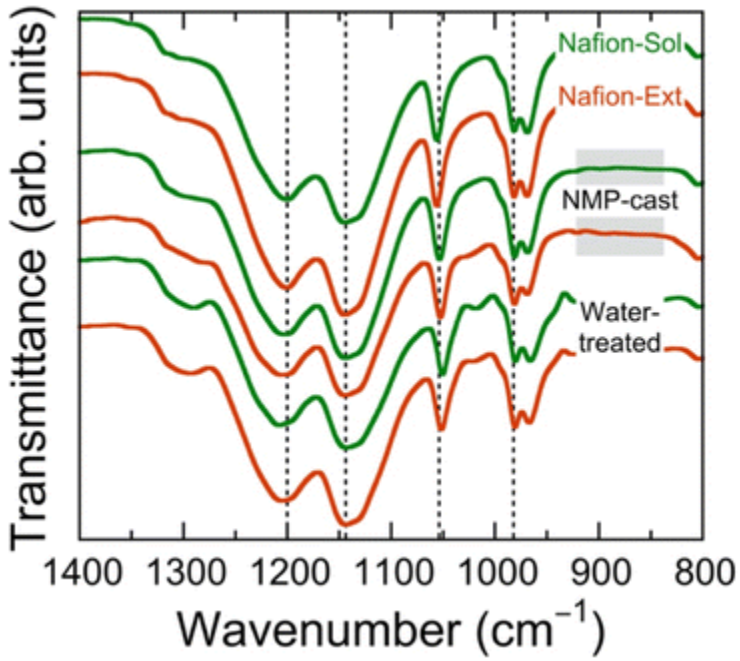

Fig. 4 FTIR spectra collected from the Nafion-Sol (green) and Nafion-Ext (orange) materials prepared in this study *via* various methods (labeled). Several principal peak wavenumbers are identified (see Table 1).

Table 1 FTIR peak assignments for Nafion

Wavenumber (cm^{-1})	**Peak assignment**	**Ref.**
969	C–O–C stretch	40
982	S–O symmetric stretch	41
1055	S–O symmetric stretch	41
1144	C–F symmetric stretch	36
1200	C–F asymmetric stretch	36
1716	H_2O and H_3O^+ bending vibrations	38
3430	H_2O and H_3O^+ stretching vibrations	36

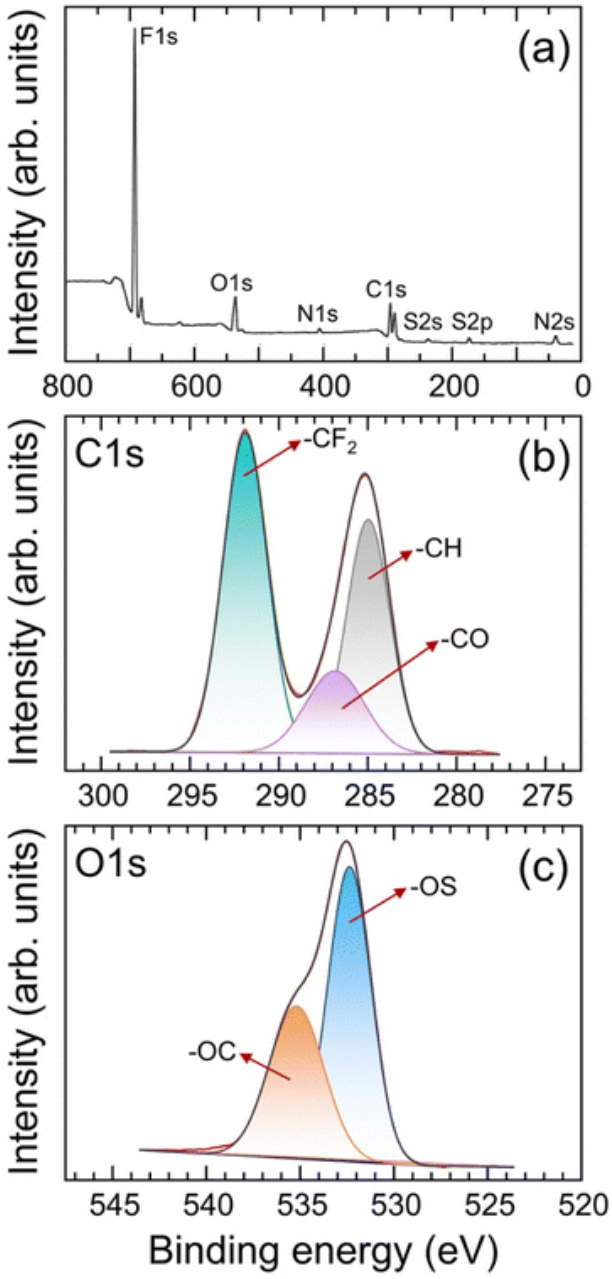

Fig. 5 XPS spectra acquired from the Nafion-Sol-water material: (a) survey spectrum and high-resolution spectra for (b) C 1s and (c) O 1s. Results from peak deconvolution of these high-resolution spectra are included (labeled and color-differentiated).

The spectrum corresponding to the C 1s region (300–275 eV) is presented in Fig. 5b and confirms the existence of three chemical functionalities, namely $–CF_2$, –CO and –CH (which overlaps with C–C), accounting for the principal carbon moieties of Nafion. The spectrum for the O 1s region in Fig. 5c consists of two different contributions (–OC and –OS), whereas the spectra acquired from the F 1s and S 2p regions are accurately described by single peaks (for –FC and –OS, respectively). All the XPS surface spectra collected here have been analyzed, and the resulting functionality composition (calculated from the peak area ratio, *A*) and binding energy (BE) values are listed in Tables 2 and 3 for each Nafion-Sol and Nafion-Ext material,

respectively. While no significant changes are apparent from these data (in agreement with the FTIR results displayed in Fig. 4), two interesting outcomes are noteworthy. The first is that the $–CF_3$ functionality is only present on the surface of the as-received Nafion-Sol polymer. In all other variations (including those derived from the Nafion-Sol material), this functionality is replaced by $–CF_2$ and –CH functionalities. The other interesting observation is that the –CO and –CS functionalities corresponding to polar bonds (that typically possess high surface energy and prefer to remain buried below the surface) within Nafion are both present on the surface of the Nafion-Sol material, but only one of the two stochastically exists on the surfaces of all the other materials examined. Another unexpected finding is that the –OS/–OC surface ratio for the Nafion-Ext-NMP polymer is much higher (~3.0) relative to all the others (1.1–1.5), suggesting that the surface of this polymer is more enriched with sulfonic acid groups.

Table 2 Chemical compositions and binding energies extracted from high-resolution XPS spectra for each of the Nafion-Sol materials investigated here

		Nafion-Sol		**Nafion-Sol-NMP**		**Nafion-Sol-water**	
Peak	**Functionality**	**BE (eV)**	***A* (%)**	**BE (eV)**	***A* (%)**	**BE (eV)**	***A* (%)**
F 1s	–FC	691.35	100	689.01	100	689.24	100
O 1s	–OS	532.21	52.11	532.17	54.78	532.33	60.38
	–OC	534.81	47.89	535.42	45.22	535.17	39.62
C 1s	$–CF_2$	—	—	291.88	44.57	291.92	48.68
	$–CF_3$	294.11	53.41	—	—	—	—
	–CH	—	—	285.16	35.59	284.92	34.72
	–CO	287.14	25.85	—	—	286.84	16.60
	–CS	288.76	25.85	290.21	19.84	—	—
S 2p	–SO	169.17	100	168.85	100	169.01	100

Table 3 Chemical compositions and binding energies extracted from high-resolution XPS spectra for each of the Nafion-Ext materials investigated here

		Nafion-Ext		**Nafion-Ext-NMP**		**Nafion-Ext-water**	
Peak	**Functionality**	**BE (eV)**	***A* (%)**	**BE (eV)**	***A* (%)**	**BE (eV)**	***A* (%)**
F 1s	–FC	689.04	100	688.57	100	689.39	100
O 1s	–OS	532.19	53.04	532.04	74.88	532.59	55.15
	–OC	534.91	46.96	535.06	25.12	535.37	44.84
C 1s	$–CF_2$	291.64	59.02	291.52	52.86	292.22	44.11
	$–CF_3$	—	—	—	—	—	—
	–CH	285.03	26.20	284.91	32.93	285.25	39.34
	–CO	286.43	14.78	287.79	14.21	—	—
	–CS	—	—	—	—	289.74	16.55

		Nafion-Ext		Nafion-Ext-NMP		Nafion-Ext-water	
Peak	**Functionality**	**BE (eV)**	***A* (%)**	**BE (eV)**	***A* (%)**	**BE (eV)**	***A* (%)**
S 2p	–SO	168.83	100	168.70	100	169.36	100

Nafion membranes are nanostructured amphiphilic copolymers due to the existence of contiguous nanoscale channels composed of hydrophilic moieties and embedded within a hydrophobic matrix.[42] As previously reported,[43] the presence of water vapor significantly affects the gas-transport characteristics of Nafion, and its CO_2 permeability can increase by about two orders of magnitude at 100% RH. During water absorption, water molecules serve to swell the nanoscale hydrophilic channels and thus enhance the permeability of gases that are highly soluble in water (*e.g.*, CO_2) without significantly benefiting those with a low solubility (*e.g.*, N_2). As indicated by the data displayed in Fig. 6a and b, all the Nafion membranes produced here swell to different extents (with Nafion-Ext possessing the greatest uptake) after exposure to water vapor for 24 h. Included in Fig. 6a, are uptake values expressed in terms of mol (H_2O) per mol(SO_3), whereas Ω values calculated according to eqn (1) are presented in Fig. 6b. A noteworthy observation is that, while Ω = 6.8% for the Nafion-Sol membrane, Ω nearly doubles upon water treatment (13.5%) or NMP casting (13.0%). Surprisingly, Nafion-Ext membranes exhibit an opposite outcome: Ω for the parent polymer is 17.5%, but this drops to 6.2% and 10.2% upon water treatment and NMP casting, respectively. Exposure of membranes measuring 2 cm × 2 cm to liquid water expectedly causes all the membranes to swell in the thickness direction. Interestingly, the Nafion-Sol membranes (as-received, water-treated and NMP-cast) undergo the greatest swelling.

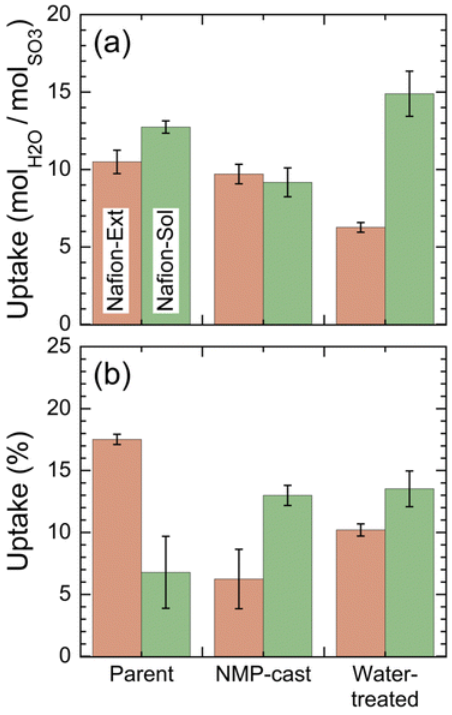

Fig. 6 (a) Water uptake and (b) water-vapor uptake of membranes derived from Nafion-Sol (green) and Nafion-Ext (orange) and prepared according to different protocols. The error bars correspond to the standard deviation.

3.3. Mixed-gas permeation

In this study, the gas-permeability characteristics of the parent Nafion-Sol and Nafion-Ext membranes have been investigated with a CO_2/N_2 gas mixture at different RH levels to elucidate the influence of water vapor on CO_2 transport. According to the measurements provided in Fig. 7a, water vapor clearly has a significant and systematic positive impact on CO_2 permeability of both Nafion membranes. As the RH is increased from 50 to 100%, the CO_2 permeability of the Nafion-Sol membrane increases from 71 to 208 Barrer, which is almost a 200% increase. A similar level of improvement is observed for the Nafion-Ext membrane. According to the SAXS profiles displayed in Fig. 2a, the nanostructure comprising the Nafion-Sol membrane do not exhibit long-range order and limited evidence of correlated ionic clusters (in contrast to the Nafion-Ext membranes in Fig. 2b). These features suggest that the nanostructure in Nafion consists of highly irregular hydrophilic channels, which is consistent with a random copolymer architecture. Such channels can help to promote the diffusion of CO_2 upon hydration, in qualitative agreement with our previous findings[18,20] from a nonequilibrated anionic block polymer immersed in water. We therefore conclude that water vapor in the gas feed can be judiciously used to improve the permeability of CO_2 in nanostructured amphiphilic polyelectrolytes such as Nafion. In contrast, however, the CO_2/N_2 selectivity increases only slightly (<32%) upon increasing the RH from 50 to 100% in Fig. 7b.

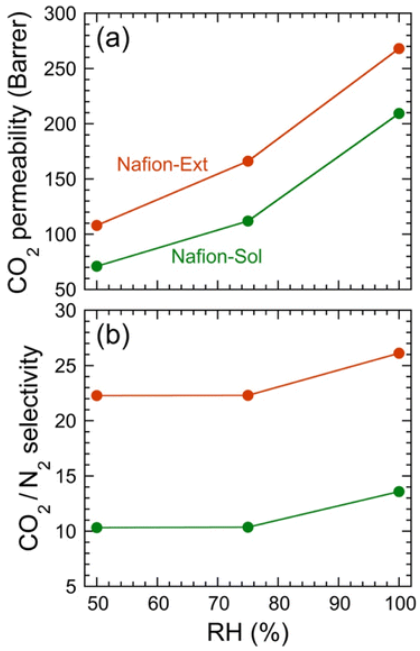

Fig. 7 Dependence of (a) CO_2 permeability and (b) CO_2/N_2 selectivity in Nafion-Sol (green) and Nafion-Ext (orange) membranes on the relative humidity (RH) of the feed gas at ambient temperature and 2.0 bar. The solid lines serve to connect the data.

Similar mixed-gas permeability tests have likewise been performed on the membranes prepared from the as-received Nafion-Sol and Nafion-Ext polymers after water treatment and NMP casting to discern the extent to which (non)solvent-induced nanostructural rearrangement influences CO_2 permeability and CO_2/N_2 separation selectivity. The results acquired at a RH level of 100% are presented in Fig. 8a and b, respectively. Upon hydration, the CO_2 permeability in the as-received Nafion membranes increases to 209 (Nafion-Sol) and 268 (Nafion-Ext) Barrer, as first established in Fig. 7a. The corresponding CO_2/N_2 selectivity levels are 13.6 and 26.1, respectively, indicating that CO_2 permeates between ~13–26× faster than N_2 due to the presence of hydrophilic nanochannels. For comparison, the CO_2/N_2 selectivity in superhydrophobic amorphous poly(tetrafluoroethylene) (PTFE AF2400) is ~7.[8] Our hypothesis here is that an increase in the connectivity of the hydrophilic nanochannels can enhance at least CO_2 permeability. The measurements provided in Fig. 8a demonstrate two different trends. The first is that the CO_2 permeability in both membranes (water-treated and NMP-cast) derived from the Nafion-Sol parent polymer increases to different degrees in the presence of water vapor at 100% RH, whereas the second is that this trend is opposite for the membranes fabricated from Nafion-Ext. This stark difference reflects the morphological and physico-chemical differences identified between the two series of materials earlier in this work, confirming that not all Nafion membranes are the same and yield identical property sets.

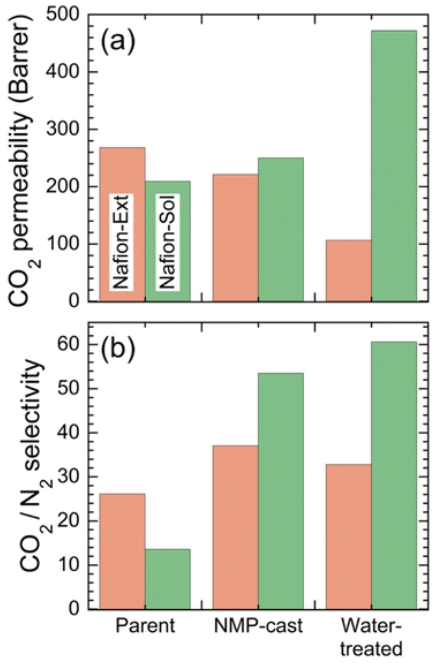

Fig. 8 (a) CO2 permeability and (b) CO2/N2 selectivity of Nafion-Sol (green) and Nafion-Ext (orange) membranes prepared according to different protocols at ambient temperature and 2.0 bar at 100% RH.

Since water vapor in the mixed-gas feed improves the gas-transport performance of the Nafion-Sol membrane series, we only consider these materials further in Fig. 8a. Although the presence of water vapor has relatively little impact on CO_2 permeability in the Nafion-Sol-NMP membrane, it more than doubles the permeability of CO_2 in the Nafion-Sol-water membrane (from 209 to 472 Barrer). This direct comparison provides compelling evidence that the hydrophilic nanochannels (swollen by water vapor) in the Nafion-Sol-water membrane are more contiguous and therefore capable of accelerating CO_2 diffusion. In contrast, the water-treated Nafion-Ext-water membranes exhibit the lowest CO_2 permeability, implying that immersion of the Nafion-Ext membrane in DI water negatively alters (possibly collapsing or contracting) the hydrophilic nanochannels. This difference in response to hydrated feed gas clearly merits further investigation into its origin. The results displayed in Fig. 8b reveal that, while the CO_2/N_2 selectivity is enhanced for the two series of membranes in the presence of 100% RH, it is much more pronounced for the Nafion-Sol-NMP and Nafion-Sol-water membranes. In the case of the water-treated membrane, the selectivity increases by more than a factor of 4×, which establishes that this membrane benefits in terms of both CO_2 permeability and CO_2/N_2 selectivity. Examples of concurrent increases in permeability and selectivity are contrary to the permeability–selectivity trade-off encountered with membranes operating by the solution-diffusion mechanism and exemplified by the upper bound on a Robeson plot.[16] Such examples do, however, exist and often indicate either a different gas-transport mechanism (*e.g.*, facilitated transport) or two different mechanisms functioning in tandem.[8]

Fig. 8 also establishes the influence of casting solvent on CO_2 transport through the Nafion membranes cast from NMP. More specifically, the CO_2 permeability and CO_2/N_2 selectivity of the Nafion-Sol-NMP membrane at 100% RH increase simultaneously to 250 Barrer and 53.5, respectively, which are less pronounced than those in the Nafion-Sol-water membrane. While

the Nafion-Ext-NMP membrane does not exhibit the same correlated behavior, the results for the Nafion-Sol-NMP membrane further indicate that (non)solvent-induced nanostructural modification can significantly improve the CO_2 permeability and CO_2/N_2 selectivity in amphiphilic polyelectrolytes such as Nafion. In addition to investigating the effect of casting solvent, we have examined CO_2 transport through these two membranes at temperatures up to 45 °C. Our findings, included in Fig. 9a for CO_2 permeability and Fig. 9b for CO_2/N_2 selectivity, indicate that the two membranes possess a markedly different dependence of permeability on temperature but relatively similar selectivity behavior. In Fig. 9a, an increase in temperature causes the permeability of CO_2 in the Nafion-Sol-NMP membrane to first plummet and then stabilize, suggesting that the solubility of CO_2 in Nafion decreases (since diffusion increases with increasing temperature). Lower CO_2 solubility at elevated temperatures further implies less water uptake, which agrees with Ω = 14.0% measured at 45 °C (compared to 16.0% at 25 °C in Fig. 6b). In contrast, the CO_2 permeability increases slightly in the Nafion-Ext-NMP membrane most likely due to higher CO_2 diffusivity. Increasing the temperature in Fig. 9b promotes selectivity reductions in both membranes, with the change in CO_2/N_2 selectivity being more prominent in the Nafion-Sol-NMP membrane.

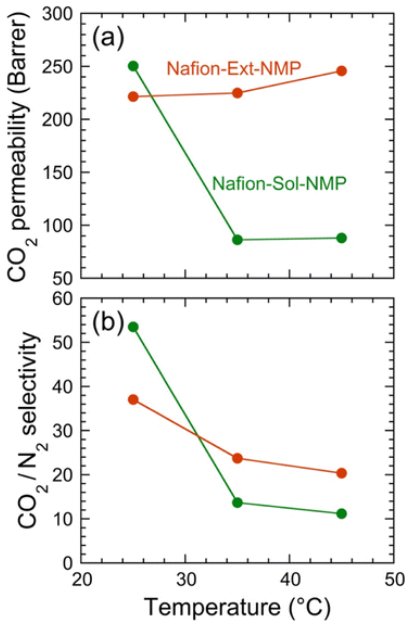

Fig. 9 (a) CO_2 permeability and (b) CO_2/N_2 selectivity of Nafion-Sol-NMP (green) and Nafion-Ext-NMP (orange) at 2.0 bar and 100% RH. The solid lines serve to connect the data.

The separation performance of the various Nafion membranes prepared in this study are compared with other perfluorinated sulfonated membranes reported elsewhere in Table 4. Aside from the results reported herein, the highest CO_2 permeability achieved is 257 Barrer,[44] and the highest CO_2/N_2 selectivity (for a different membrane) is only 15.0,[27] in which case the separation properties of the Nafion-Sol-water membrane produced here (with attributes of 472 Barrer and 60.6, respectively) are not only far superior to those of any previous Nafion-based membranes but also competitive relative to many carbon-capture membranes that operate by the solution-diffusion mechanism. Of equal importance is our largely unexplored

approach to controlling CO_2 molecular transport *via* only nanostructural modification. To ascertain the efficacy of our Nafion-based membranes in relation to the 2008 and 2019 upper bounds,[16,45] we present our permeability and selectivity findings in a Robeson-style plot in Fig. 10. According to this representation, CO_2 transport in the Nafion-Sol membrane is so significantly improved after immersion in DI water that its performance clearly surpasses the 2008 upper bound and approaches the 2019 upper bound, which was introduced to account for a family of membranes fabricated from polymers of intrinsic microporosity (PIMs). Even when the Nafion-Sol membrane is cast from NMP, its separation performance surpasses that of the Nafion-Ext-NMP membrane and comes close to the 2008 upper bound. Along with most polymer membranes intended for carbon capture, the remaining membranes derived from, and including, the Nafion-Sol and Nafion-Ext polymers all lie below the 2008 upper bound.

Table 4 Separation performance of selected perfluorosulfonated membranes and Nafion membranes prepared according to different protocols

Membrane	***P*** **$_{CO2}$ (Barrer)**	**CO_2/N_2 selectivity**	**Ref.**
Nafion N117 (dry)	2.3	9.6	46
Nafion D520 (dry)	1.6	8.7	47
Nafion D520 (50% RH)	71	10.8	47
Nafion D520 (100% RH)	209	14.8	47
Nafion D520 (dry)	1.6	8.9	27
Nafion D520 (100% RH)	209	15.0	27
Nafion N111 (dry)	2.3	—	44
Nafion N111 (100% RH)	257	—	44
Nafion-Sol (50% RH)	71	10.3	This work[c]
Nafion-Sol (100% RH)	209	13.6	This work[c]
Nafion-Ext (50% RH)	108	22.3	This work[c]
Nafion-Ext (100% RH)	268	26.1	This work[c]
Nafion-Sol-NMP (100% RH)	250	53.5	This work[c]
Nafion-Ext-NMP (100% RH)	221	37.1	This work[c]
Nafion-Sol-water (100% RH)	472	60.6	This work[c]
Nafion-Ext-water (100% RH)	106	32.8	This work[c]

a **Single-gas permeation test, feed pressure of 2 bar at 35 °C.** ***b*** **Mixed-gas permeation test, feed pressure of 2 bar at 35 °C.** ***c*** **Mixed-gas permeation test, feed pressure of 2 bar at ambient temperature.** ***d*** **Single-gas permeation test, feed pressure of 1 bar at 25 °C.**

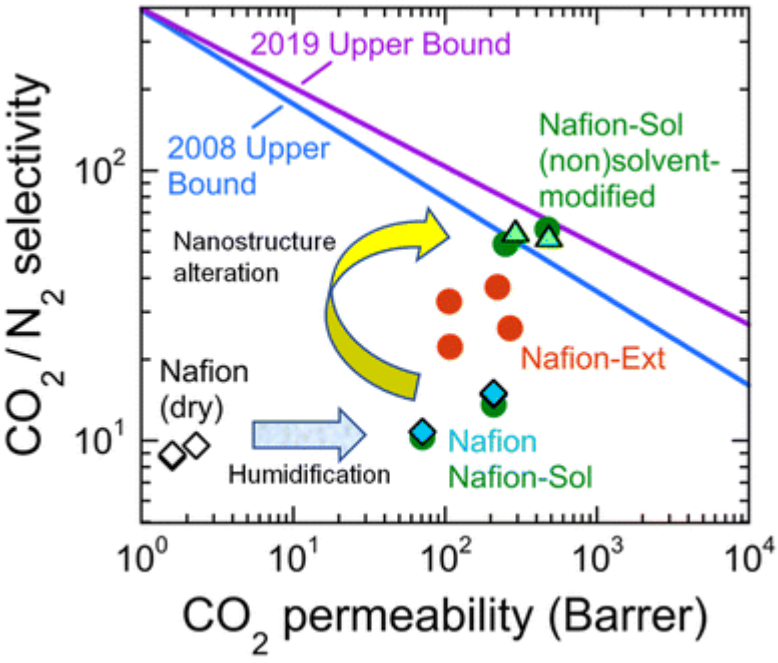

Fig. 10 Robeson plot displaying the CO2 separation performance measured from mixed-gas permeation tests of Nafion membranes prepared here according to different protocols (circles; labeled and color-coded). Literature values are included for comparison (diamonds), and the 2008 and 2019 upper bounds are identified. Also provided are results from a midblock-sulfonated pentablock polymer18 subjected to nonsolvent (water) treatment (triangles).

4. Conclusions

In summary, we have subjected a nanostructured amphiphilic polyelectrolyte (Nafion) to either a solvent (NMP) or a non-solvent (water) with the intention of altering the nanostructural characteristics to improve the permeability and selectivity of CO_2 for carbon capture. To this end, we have considered two different Nafion variants, one prepared from solution (Nafion-Sol) and the other from melt extrusion (Nafion-Ext). We have examined the morphologies of the resultant membranes by TEM and SAXS, and identified both similarities and important differences. Most importantly, the membranes derived from the parent Nafion-Ext polymer display sharp scattering peaks associated with ionic clusters, whereas those prepared from the Nafion-Sol polymer do not, suggesting that the Nafion-Ext membranes possess more or better defined clusters and are therefore more physically crosslinked. According to TGA, the thermal decomposition behavior of the materials, while appearing generally comparable, exhibits noticeable differences for those exposed to either solvent or nonsolvent. Similar process-related variations are observed in two ionization energies from XPS analysis of the membrane surfaces. Whereas CO_2 permeability in the parent polymers is significantly enhanced when the mixed-gas feed is fully hydrated (100% RH), the corresponding increase in CO_2/N_2 selectivity is much more modest. When the Nafion-Sol polymer is subjected to immersion in the nonsolvent, however, the CO_2 permeability and CO_2/N_2 selectivity in the resultant membrane are significantly improved by 126% and 132%, respectively. These results demonstrate that the nanostructure of amphiphilic polyelectrolytes such as Nafion™ can be altered through the use

of (non)solvents to enhance CO_2 permeability and selectivity. In the case of nonsolvent (water) treatment, this process strategy is eco-friendly, efficient and facile, providing a new materials design paradigm for more efficient CO_2 capture technology, as well as insight into nonequilibrium nanostructure transformations.

Conflicts of interest

There are no conflicts to declare.

Acknowledgements

This work was supported by the Sichuan Science and Technology Program (2021YFH0116) and the National Natural Science Foundation of China (No. 52170112).

References

1. N. Xu, X. Li, M. A. Franks, H. Zhao and K. Huang, Silver-molten carbonate composite as a new high-flux membrane for electrochemical separation of CO2 from flue gas, J. Membr. Sci., 2012, 401, 190–194 . .
2. T. C. Merkel, H. Lin, X. Wei and R. Baker, Power plant post-combustion carbon dioxide capture: An opportunity for membranes, J. Membr. Sci., 2010, 359, 126–139 . .
3. E. Favre, Carbon dioxide recovery from post-combustion processes: can gas permeation membranes compete with absorption?, J. Membr. Sci., 2007, 294, 50–59 . .
4. L.-X. Ren, F.-L. Chang, D.-Y. Kang and C.-L. Chen, Hybrid membrane process for post-combustion CO2 capture from coal-fired power plant, J. Membr. Sci., 2020, 603, 118001 . .
5. D. F. Sanders, Z. P. Smith, R. Guo, L. M. Robeson, J. E. McGrath, D. R. Paul and B. D. Freeman, Energy-efficient polymeric gas separation membranes for a sustainable future: A review, Polymer, 2013, 54, 4729–4761 . .
6. L. Shao, B. T. Low, T.-S. Chung and A. R. Greenberg, Polymeric membranes for the hydrogen economy: contemporary approaches and prospects for the future, J. Membr. Sci., 2009, 327, 18–31 . .
7. H. B. Park, J. Kamcev, L. M. Robeson, M. Elimelech and B. D. J. S. Freeman, Maximizing the right stuff: The trade-off between membrane permeability and selectivity, Science, 2017, 356, eaab0530 . . .
8. M. Sandru, E. M. Sandru, W. F. Ingram, J. Deng, P. M. Stenstad, L. Deng and R. J. J. S. Spontak, An integrated materials approach to ultrapermeable and ultraselective CO2 polymer membranes, Science, 2022, 376, 90–94 . . .
9. S. M. Cakić, I. S. Ristić, I. Krakovský, D. T. Stojiljković, P. Bělský and L. Kollová, Crystallization and thermal properties in waterborne polyurethane elastomers: Influence of mixed soft segment block, Mater. Chem. Phys., 2014, 144, 31–40 . .

10. A. Fallahi, G. Guldentops, M. Tao, S. Granados-Focil and S. Van Dessel, Review on solid-solid phase change materials for thermal energy storage: Molecular structure and thermal properties, Appl. Therm. Eng., 2017, 127, 1427–1441 . .
11. S. Luo, K. A. Stevens, J. S. Park, J. D. Moon, Q. Liu, B. D. Freeman and R. Guo, Highly CO2-selective gas separation membranes based on segmented copolymers of poly (ethylene oxide) reinforced with pentiptycene-containing polyimide hard segments, ACS Appl. Mater. Interfaces, 2016, 8, 2306–2317 . . .
12. J. S. Louie, I. Pinnau, I. Ciobanu, K. P. Ishida, A. Ng and M. Reinhard, Effects of polyether–polyamide block copolymer coating on performance and fouling of reverse osmosis membranes, J. Membr. Sci., 2006, 280, 762–770 . .
13. S. Ahmad, S. Lian, Y. Tan, R. Li, Q. Zhao, C. Song, Q. Liu and S. J. Lu, Solvent influence on the textural properties and CO2/N2 separation performance of novel Pebax-1657/attapulgite mixed matrix membranes, J. Environ. Chem. Eng., 2021, 9, 105806 . .
14. W. Yave, A. Szymczyk, N. Yave and Z. Roslaniec, Design, synthesis, characterization and optimization of PTT-b-PEO copolymers: A new membrane material for CO2 separation, J. Membr. Sci., 2010, 362, 407–416 . .
15. M. Karunakaran, R. Shevate, M. Kumar and K.-V. Peinemann, CO2-selective PEO–PBT (PolyActive™)/graphene oxide composite membranes, Chem. Commun., 2015, 51, 14187–14190.
16. L. M. Robeson, The upper bound revisited, J. Membr. Sci., 2008, 320, 390–400 . .
17. H. Mizuno, K. Hashimoto, R. Tamate, H. Kokubo, K. Ueno, X. Li and M. Watanabe, Microphase-separated structures of ion gels consisting of ABA-type block copolymers and an ionic liquid: A key to escape from the trade-off between mechanical and transport properties, Polymer, 2020, 206, 122849 . .
18. Z. Dai, J. Deng, H. Aboukeila, J. Yan, L. Ansaloni, K. P. Mineart, M. Giacinti Baschetti, R. J. Spontak and L. Deng, Highly CO2-permeable membranes derived from a midblock-sulfonated multiblock polymer after submersion in water, NPG Asia Mater., 2019, 11, 53 . .
19. K. P. Mineart, X. Jiang, H. Jinnai, A. Takahara and R. J. J. M. R. C. Spontak, Macromol. Rapid Commun., 2015, 36, 432–438 . . .
20. K. P. Mineart, H. A. Al-Mohsin, B. Lee and R. J. Spontak, Water-induced nanochannel networks in self-assembled block ionomers, Appl. Phys. Lett., 2016, 108, 101907 . .
21. Z. Dai, L. Ansaloni, J. J. Ryan, R. J. Spontak and L. Deng, Incorporation of an ionic liquid into a midblock-sulfonated multiblock polymer for CO2 capture, J. Membr. Sci., 2019, 588, 117193 . .
22. M. A. Yandrasits, M. J. Lindell and S. J. Hamrock, New directions in perfluoroalkyl sulfonic acid–based proton-exchange membranes, Curr. Opin. Electrochem., 2019, 18, 90–98 . .
23. F. I. Allen, L. R. Comolli, A. Kusoglu, M. A. Modestino, A. M. Minor and A. Z. Weber, Morphology of hydrated as-cast Nafion revealed through cryo electron tomography, ACS Macro Lett., 2015, 4, 1–5 . . .
24. K. A. Mauritz and R. B. Moore, State of understanding of Nafion, Chem. Rev., 2004, 104, 4535–4585 . . .

25. S. Quezado, J. C. Kwak and M. Falk, An infrared study of water–ion interactions in perfluorosulfonate (Nafion) membranes, Can. J. Chem., 1984, 62, 958–966 . .
26. Z. Dai, H. Aboukeila, L. Ansaloni, J. Deng, M. G. Baschetti and L. Deng, Nafion/PEG hybrid membrane for CO2 separation: Effect of PEG on membrane micro-structure and performance, Sep. Purif. Technol., 2019, 214, 67–77 . .
27. Z. Dai, L. Ansaloni, J. J. Ryan, R. J. Spontak and L. J. Deng, Nafion/IL hybrid membranes with tuned nanostructure for enhanced CO2 separation: Effects of ionic liquid and water vapor, Green Chem., 2018, 20, 1391–1404
28. T. Xue, J. S. Trent and K. Osseo-Asare, Characterization of Nafion® membranes by transmission electron microscopy, J. Membr. Sci., 1989, 45, 261–271 . .
29. F. Yang, L. Xin, A. Uzunoglu, Y. Qiu, L. Stanciu, J. Ilavsky, W. Li and J. Xie, Investigation of the Interaction between Nafion Ionomer and Surface Functionalized Carbon Black Using Both Ultrasmall Angle X-ray Scattering and Cryo-TEM, ACS Appl. Mater. Interfaces, 2017, 9, 6530–6538 . . .
30. K. Karan, Interesting Facets of Surface, Interfacial, and Bulk Characteristics of Perfluorinated Ionomer Films, Langmuir, 2019, 35, 13489–13520 . . .
31. K. D. Kreuer and G. J. A. F. M. Portale, A critical revision of the nano-morphology of proton conducting ionomers and polyelectrolytes for fuel cell applications, Adv. Funct. Mater., 2013, 23, 5390–5397 . .
32. W. Zhang, P.-L. Yue and P. Gao, Crystallinity Enhancement of Nafion Electrolyte Membranes Assisted by a Molecular Gelator, Langmuir, 2011, 27, 9520–9527 .
33. D. J. Yarusso and S. L. Cooper, Microstructure of ionomers: interpretation of small-angle x-ray scattering data, Macromolecules, 1983, 16, 1871–1880 . .
34. Q. Deng, C. Wilkie, R. Moore and K. A. Mauritz, TGA–FTi. r. investigation of the thermal degradation of Nafion® and Nafion®/[silicon oxide]-based nanocomposites, Polymer, 1998, 39, 5961–5972 . .
35. S. De Almeida and Y. Kawano, Thermal behavior of Nafion membranes, J. Therm. Anal. Calorim., 1999, 58, 569–577 . .
36. J. Ostrowska and A. Narębska, Infrared study of hydration and association of functional groups in a perfluorinated Nafion membrane – Part 2, Colloid Polym. Sci., 1984, 262, 305–310 . .
37. W. Kujawski, Q. T. Nguyen and J. Neel, Infrared investigations of sulfonated ionomer membranes. I. Water–alcohol compositions and counterions effects, J. Appl. Polym. Sci., 1992, 44, 951–958 . .
38. M. Laporta, M. Pegoraro and L. Zanderighi, Perfluorosulfonated membrane (Nafion): FT-IR study of the state of water with increasing humidity, Phys. Chem. Chem. Phys., 1999, 1, 4619–4628.
39. M. Vijayakumar, M. Bhuvaneswari, P. Nachimuthu, B. Schwenzer, S. Kim, Z. Yang, J. Liu, G. L. Graff, S. Thevuthasan and J. Hu, Spectroscopic investigations of the fouling process on Nafion membranes in vanadium redox flow batteries, J. Membr. Sci., 2011, 366, 325–334 . .
40. H. Matsuura, T. Miyazawa and K. Machida, Infrared spectra of poly (ethylene glycol) dimethyl ethers in the crystalline state, Spectrochim. Acta, Part A, 1973, 29, 771–779 . .

41. J. Ostrowska and A. Narebska, Infrared study of hydration and association of functional groups in a perfluorinated Nafion membrane, Part 1, Colloid Polym. Sci., 1983, 261, 93–98 . .
42. H.-Y. Jung, M.-S. Cho, T. Sadhasivam, J.-Y. Kim, S.-H. Roh and Y. Kwon, High ionic selectivity of low permeable organic composite membrane with amphiphilic polymer for vanadium redox flow batteries, Solid State Ionics, 2018, 324, 69–76 . .
43. M. G. Baschetti, M. Minelli, J. Catalano and G. C. Sarti, Gas permeation in perflurosulfonated membranes: Influence of temperature and relative humidity, Int. J. Hydrogen Energy, 2013, 38, 11973–11982 . .
44. S. Ma and E. Skou, CO2 permeability in Nafion® EW1100 at elevated temperature, Solid State Ionics, 2007, 178, 615–619 . .
45. B. Comesaña-Gándara, J. Chen, C. G. Bezzu, M. Carta, I. Rose, M.-C. Ferrari, E. Esposito, A. Fuoco, J. C. Jansen and N. B. McKeown, Redefining the Robeson upper bounds for CO2/CH4 and CO2/N2 separations using a series of ultrapermeable benzotriptycene-based polymers of intrinsic microporosity, Energy Environ. Sci., 2019, 12, 2733–2740 .
46. M. Mukaddam, E. Litwiller and I. Pinnau, Gas sorption, diffusion, and permeation in Nafion, Macromolecules, 2016, 49, 280–286 . .
47. Z. Dai, H. Aboukeila, L. Ansaloni, J. Deng, M. G. Baschetti, L. J. S. Deng and P. Technology, Nafion/PEG hybrid membrane for CO2 separation: Effect of PEG on membrane micro-structure and performance, Sep. Purif. Technol., 2019, 214, 67–77